Impact of Porous Electrode Properties on the Electrochemical Transfer Coefficient

Jeff N. Soderberg, Anne C. Co, Aislinn H. C. Sirk, and Viola I. Birss*

Department of Chemistry, University of Calgary, 2500 University Drive, N.W., Calgary, AB, Canada T2N 1N4

Received: January 18, 2006; In Final Form: March 14, 2006

The rate of an activation-controlled electrochemical reaction is determined by two key parameters, the exchange current density, i_o, and the transfer coefficient, α, which is inversely related to the Tafel slope. Assuming that the symmetry factor, β, is 0.5, the minimum α value should be 0.5 for all standard reaction mechanisms, with α values larger than this indicating a better electrocatalytic mechanism. The primary goal of this paper is to better understand why α values of <0.5 are often observed experimentally, with specific examples given for the oxygen reduction reaction. These low α values cannot be explained by adsorption behavior, but they can result when reactions occur within a porous electrode structure. Consistent with past literature related to Tafel slope predictions, we show that long and narrow pores, a low ionic or electronic conductivity of the electrode layer, and a high i_o value can cause α to be <0.5, most typically 0.25. However, α values between 0.25 and 0.5 are also encountered in practice. We show here that such α values can be obtained for reactions occurring at porous films that have nonuniform properties. We also show that the overpotential range over which α changes from 0.5 to 0.25 can be quite broad, especially at high temperatures, and thus can be misinterpreted as a true Tafel region with a transfer coefficient between 0.25 and 0.5.

Introduction

The desire to control the rate of electrochemical reactions is relevant to many practical applications. These include increasing the rate of the conversion of water to hydrogen and oxygen, chlorine evolution from brine solutions, metal electrowinning processes, organic electrosyntheses, reactions in battery and fuel cell devices, and decreasing the rate of metal corrosion. The most important relationship governing electrochemical reaction rates is the Butler−Volmer (BV) equation (eq 1), which provides the fundamental kinetic relationship between the current density (the reaction rate), i, and the overpotential, η, applicable when the rate is controlled by the charge-transfer process (activation controlled reactions).

$$i = i_o\left(\exp\left(\frac{\alpha_a F}{RT}\eta\right) - \exp\left(\frac{-\alpha_c F}{RT}\eta\right)\right) = i_o\left(\exp\left(\frac{2.303\eta}{b_a}\right) - \exp\left(\frac{-2.303\eta}{b_c}\right)\right) \quad (1)$$

The two key parameters that influence i are the exchange current density, i_o, and the transfer coefficient, α, which can be experimentally obtained from the Tafel slope, b, where R, T, and F have their usual thermodynamic meanings and subscripts "a" and "c" refer to anodic and cathodic reactions, respectively.[1,2]

$$b = \frac{2.303RT}{\alpha F} \quad (2)$$

i_o reflects the inherent rate of the rate-determining step of an electrochemical reaction, and its magnitude depends on the concentration and order of the reactants and the temperature. i_o can be determined from the low- and/or high-field analysis of the BV equation or from the charge-transfer resistance measured using electrochemical impedance spectroscopy.[3]

TABLE 1: Predicted α_{mech} Values[a] for Hypothetical Electrochemical Reaction Mechanism[b]

$A + 4e^- \rightarrow F$	rate determining step	β	α_{mech}
$A \rightarrow B$	step 1	n/a	0
$B + e^- \rightarrow C$	step 2	0.5	0.5
$C + e^- \rightarrow D$	step 3	0.5	1.5
$D \rightarrow 2E$	step 4	n/a	2
$2(E + e^- \rightarrow F)$	step 5	0.5	1.5

[a] From eq 3. [b] Assuming no adsorption effects and that $\beta = 0.5$ for all electron-transfer steps.

The Tafel slope, b (eq 2), is proportional to $1/\alpha$, where α is the fraction of potential energy that is transferred to the reaction. When α is predicted from a particular reaction mechanism, we define it as α_{mech}[4]

$$\alpha_{mech} = \frac{\gamma}{\nu} + r_{rds}\beta \quad (3)$$

where γ is the number of electrons preceding the rate-determining step (rds), ν is the number of occurrences of the rds, r_{rds} is the number of electrons passed in the rds, and β is the symmetry factor.[1] At room temperature, when β is 0.5 (its most common value), and ignoring adsorption effects, the lowest expected α_{mech} value is 0.5 and the highest b value is then 118 mV. Table 1 shows the α_{mech} values predicted for various slow steps in a hypothetical electrochemical reaction, while Table 2 gives the b values that would be expected for different α_{mech} values as a function of temperature.

While α_{mech} values can clearly be >0.5 (Table 1 and eq 3), experimentally obtained α values are sometimes <0.5, even as low as 0.25 or less. Clearly, these low values are not predicted by conventional mechanistic analysis. This paper is directed specifically toward understanding the possible origins of these

* To whom all correspondence should be addressed. Phone: (403) 220-6432. Fax: (403) 284-9488. E-mail: birss@ucalgary.ca.

10.1021/jp060372f CCC: $33.50
Published on Web 05/10/2006

TABLE 2: Predicted Tafel Slope Values[a] for Given α_{mech} Values at Various Temperatures[b]

	Tafel slope (*b*) (mV/decade current)				
α_{mech} value	25 °C	200 °C	400 °C	600 °C	800 °C
1	59.1	93.8	133.4	173.1	212.7
0.5	118.2	187.6	266.8	346.1	425.4
0.25	236.4	375.1	533.7	692.2	850.8

[a] From eq 1. Error in Tafel Slope values due to rounding are (±0.05). [b] Assuming that $\beta = 0.5$.

low α values of <0.5, including when α is halved (*b*, the Tafel slope, is doubled) for the case when the first electron-transfer step is rate-limiting (i.e., $\alpha_{mech} = 0.5$). This situation has been shown previously in the literature[5−12] to arise in special cases involving porous electrode structures. More importantly, we provide here some new insights regarding the case when Tafel slopes are between their normal and doubled values (α between 0.25 and 0.5).

The specific experimental focus of this paper is on the oxygen reduction reaction (ORR) under conditions applicable to low-temperature proton exchange membrane fuel cells (PEMFCs) and high-temperature solid oxide fuel cells (SOFCs). All of the experimental *i*/*E* data examined here have been corrected to remove the effect of the high frequency series resistance from the data, and only Tafel slopes that satisfied our criteria (linear over at least 1 order of magnitude of current and giving an excellent correlation, with $r^2 > 0.99$) were analyzed in this work. It is also assumed for the purpose of this analysis that $\beta = 0.5$, as is often found to be the case, and only the situation of α values ≤0.5 are examined in this work. It will be shown that, using known porous electrode models and reasonable estimations of the pore length, radius, and conductivity, as well the catalytic activity of the electrode, it is possible to obtain α values between 0.25 and 0.5 (or Tafel slopes of greater than 118 mV at 25 °C). Under these conditions, it is not possible to establish the mechanism of an electrochemical reaction using normal Tafel slope analysis.

Experimental Methods

1. Preparation of LSM−YSZ Cathodes for Solid Oxide Fuel Cells. $(La_{0.8}Sr_{0.2})_{0.98}MnO_3$ (LSM)−8 mol % Y_2O_3 doped ZrO_2 (LSM−YSZ) composites (1:1.75 mol ratio) were prepared either by Versa Power Systems (for the purpose of this project) or in-house, using commercial powders (Praxair Ceramics Inc., Seattle). Briefly,[3,13] a LSM−YSZ slurry was screen-printed symmetrically on each side of a YSZ plate and then dried at 80 °C for 15 min, after which pure LSM paste was applied to both outer surfaces to serve as the current collectors. Versa prepared cells were then sintered at 1100 °C for 2 h to provide good adhesion to the YSZ substrate, whereas in-house cells were sintered at 1100 °C for 2 h before and after the application of the LSM current collector. The LSM−YSZ electrodes later served as the working (WE) and counter (CE) electrodes. Pt paste (Ferro 4082) was then applied to the YSZ plate on the same side as the WE, to serve as a reference electrode (RE).[14] Half-cell oxygen reduction (ORR) experiments were carried out at 800 °C in a tube furnace (Lindberg). Cyclic voltammetry (CV) measurements were performed using a Solartron 1287 interface, with control and data collection handled by Corrware software (ver 2.7a).

2. Preparation of Co/N/C-Based Oxygen Reduction Cathodes for PEM Fuel Cells. The synthesis methods used for the preparation of these low-temperature ORR catalysts are discussed in detail elsewhere.[15] Briefly, ethylenediamine (en) or phenylenediamine (phen) ligands were added to a Co oxide sol, in various ratios, over several days, followed by adsorption onto C powder and heat treatment for 2 h in a N_2 atmosphere at 500−900 °C. The particle size of these catalysts was reduced[16] by mortar and pestle grinding, sonication in ethanol for 2 h, or cryogrinding under liquid nitrogen. This powder was later mixed with a solution of 1% Nafion in ethanol and applied to the surface of a glassy carbon (GC) electrode by micropipet. The ORR activity was determined using CV in an O_2 purged 0.5 M H_2SO_4 solution at 25 °C. CVs (10 mV/s) were run at various GC electrode rotation rates using an analytical rotator (Pine model ASR-2). Measurements were carried out with an EG&G PARC 175 function generator in conjunction with a Hokuto Denko HA-301 potentiostat, with data recorded using Chart 4 by PowerLab.

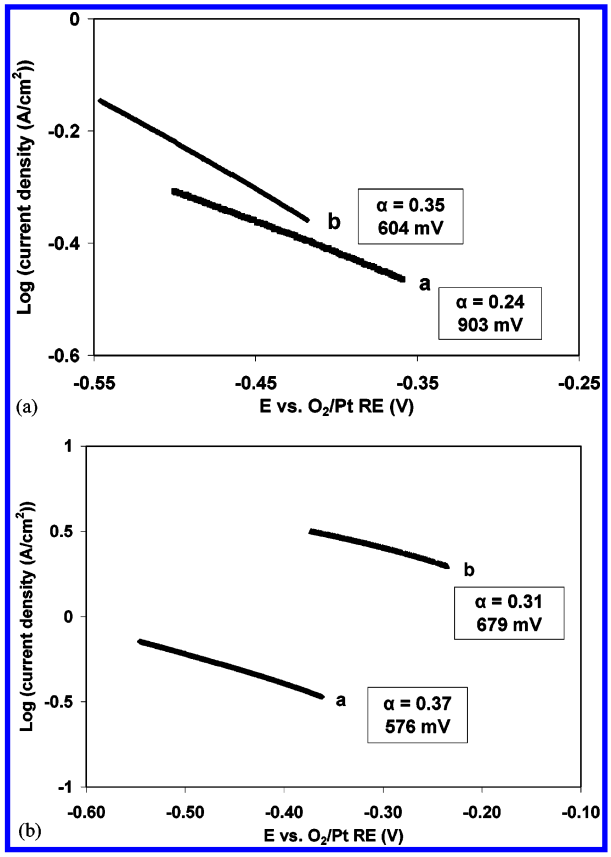

Figure 1. IR-corrected log *i*/E plot (10 mV/s) of the ORR at 800 °C in nonflowing air. (a) Effect of porosity on Tafel slope: a, in-house LSM−YSZ (10−20% porosity); b, Versa-prepared LSM−YSZ (20−30% porosity). (b) Effect of film thickness (pore length) of Versa LSM−YSZ composite cathode on Tafel slope: a, 10 μm; b, 15 μm.

3. Scanning Electron Microscopy (SEM). The thickness and porosity of the LSM−YSZ and Co/N/C catalysts were determined using a Philips/FEI environmental scanning electron microscope (Health Sciences Centre, University of Calgary). An accelerating voltage of 20 kV and a high vacuum of 2×10^{-4} Torr were generally employed. The cathodes were mechanically fractured before mounting them on Al stubs using conducting carbon tape (E. T. Enterprises). A thin layer of Au/Pd, Pt, or C was sometimes sputtered onto the sample to improve surface conductivity.

Results and Discussion

1. Oxygen Reduction Reaction Tafel Data (Examples of α < 0.5). Figure 1 shows a set of IR-corrected Tafel plots for the oxygen reduction reaction at in-house and Versa-prepared

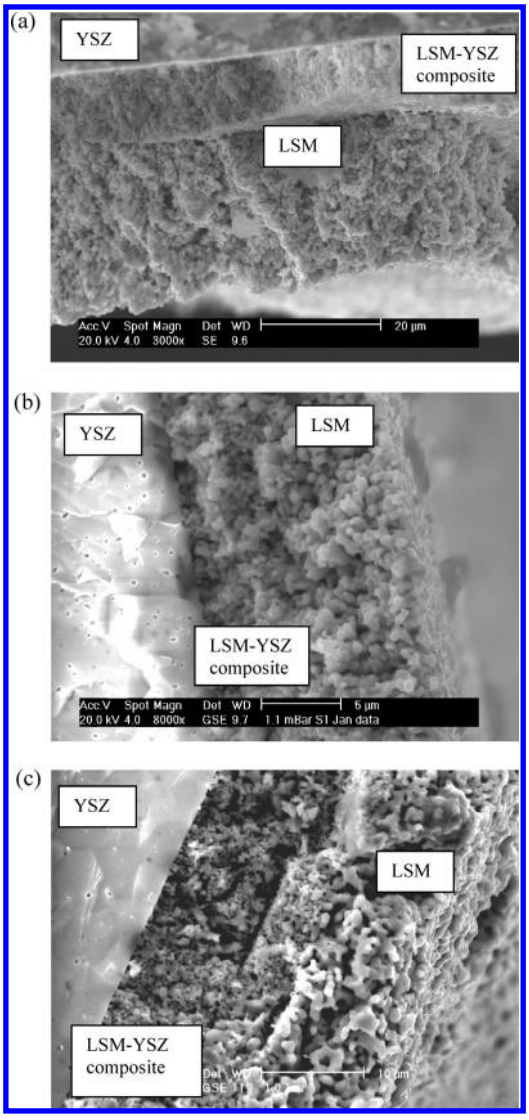

Figure 2. Cross-sectional SEM secondary electron image of (a) in-house prepared LSM−YSZ cathode, (b) Versa-supplied LSM−YSZ composite cathode layer with overlying LSM current collector, and (c) two layers of Versa-supplied LSM−YSZ composite and overlying LSM current collector, all deposited on a dense YSZ electrolyte disk.

LSM−YSZ composite cathodes at 800 °C in air as a function of porosity (controlled by a proprietary binding reagent) and electrode layer thickness (pore length). Figure 1a shows that lower porosity cathode layers (smaller pores) give lower α values and lower currents overall, while the more porous Versa-prepared cathodes are more active, as expected, but give a larger α (smaller Tafel slope, *b*). Figure 2 confirms that the pore sizes range from 0.2 to 0.65 μm for the in-house LSM−YSZ composite layer (Figure 2a), compared to 0.4−1.6 μm for the more active Versa prepared electrode (Figure 2b). The smaller pore size correlates with the very low α values of 0.2−0.25 seen at all potentials (Figure 1), while the larger pores give higher α values, 0.25−0.35, especially at high overpotentials.

The effect of pore length was examined by varying the active LSM−YSZ layer thickness, determined by SEM (Figure 2b,c). Figure 1b shows that, while a thicker cathode layer (longer pores) gives significantly higher activities, as expected, the α value decreases. It should be noted that, for all of the data in Figure 1, the *i*/*E* data were independent of potential sweep rate or oxygen gas flow rate, thus ruling out any diffusion limitations in the ORR under these conditions.

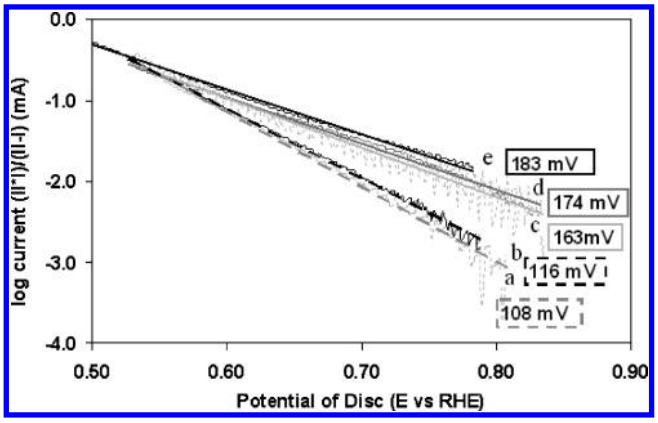

Figure 3. Tafel plot (10 mV/s) showing the effect of catalyst preparation methods, intended to decrease particle size in sequence of curves a−e, on the ORR activity of ethylenediamine-derived 20% Co/C catalyst on glassy carbon (RDE, 1000 rpm) in O_2-saturated 0.5 M H_2SO_4 at room temperature: a, mortar and pestle (I); b, mortar and pestle (II); c, sonicated 2 h; d, cryogrind (I); e, cryogrind (II).

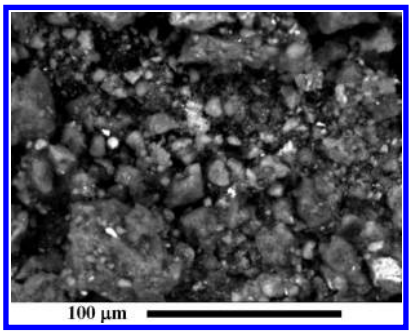

Figure 4. Composite microprobe image of mortar and pestle prepared ethylenediamine-derived 20% Co/C oxygen reduction catalyst.

Figure 3 shows some Tafel data at 25 °C for the ORR at Co/N/C catalyst materials targeted for PEM fuel cells. In this work,[17] efforts were made to change the catalyst particle size (and hence pore size) by varying the powder processing methods used. Mortar and pestle (I) preparation (curve a) involved 1 min of grinding using a mortar and pestle (further grinding of the particles showed no change in the electrochemistry). Cryogrind I and II both involved grinding of the catalyst for 5 min under liquid nitrogen using a mortar and pestle. It can clearly be seen that, as the particle size (and hence pore diameter) decreases, a notable increase in ORR activity is observed, due to the overall increased catalyst surface area. However, the Tafel slope increases (decrease in α) from 108 to 183 mV. Figure 4 shows an SEM image of the Co/N/C catalyst prepared by mortar and pestle, highlighting the nonuniformity of the particle sizes (5−50 μm) and their distribution, which will be important later in this paper.

2. Explanations for α < 0.5.

2.1. Surface Coverage Models Involving Adsorbed Reactants/Intermediates. It is well-known[16−18] that α values can be half of their predicted values (giving doubled Tafel slopes) when reactants or intermediates adsorb according to particular isotherms (e.g., Langmuir, Temkin) on electrode surfaces. However, in parallel work,[18] we have shown that, at nonporous electrodes, doubling of the Tafel slope can occur only when the rate-determining step (rds) is a reaction that occurs in a step following the first electron transfer (ET) step (Table 1). For example, a predicted 59 mV slope at 25 °C (α = 1, Table 1), associated with a slow chemical step after a first rapid ET step, will double to 118 mV (α = 0.5) when Temkin or Frumkin adsorption conditions pertain.[18] Thus, the highest Tafel slope

expected at room temperature, when $\beta = 0.5$, continues to be 118 mV and the lowest α value will be 0.5 under these adsorption conditions. α values of <0.5, which are the focus of the present work and are shown in the data of Figures 1 and 3, cannot be explained by these adsorption arguments.

2.2. Effect of Electrode Porosity. While it is well-known that a particular type of electrode porosity can lead to "doubled Tafel slopes" (halved α values), we provide below some new insights into the precise effect of electrode properties (pore dimensions, surface film conductivity, etc.) as well as temperature on these electrochemical parameters. As well, we explain how α values that are between their normal (predicted) and halved values can be obtained.

2.2.1. Doubled Tafel Slopes ($\alpha = 0.25$). A number of previous theoretical analyses have shown that porous electrode structures can lead to a doubling of the Tafel slope, e.g., when the first ET step is slow and $\beta = 0.5$, $\alpha = 0.25$ instead of 0.5.[5−12] This can arise from limitations either in the electronic or ionic conductivity of the electrode or electrolyte layers, respectively, or from mass transport limitations within the porous electrode structure. While most porous electrodes encountered in practice will contain a complex variety of structures and morphologies, the literature has focused on establishing the expected electrochemical behavior of an ideal porous electrode structure, using homogeneous and statistical models of two-phase (liquid−solid) and three-phase (gas−liquid−solid) systems. The homogeneous model[9,12] involves a macroscopic approach, considering the porous material as a series of complicated, interlinked pores, and only a specific internal area (i.e., porosity) is assumed. The statistical model[1,5,6,10,11] assumes that one pore represents an average of the entire porous layer, allowing the determination of the effect of parameters, such as pore radius and length, on the Tafel slope.

These previous approaches[1,5,6,9−12] have considered the specific cases of activation−ohmic controlled (ionic/electronic transport limitations) and activation−concentration controlled (diffusion limitations) reactions. Perry et al.[9] used a (homogeneous) flooded-agglomerate model of a gas diffusion porous electrode to examine the mass-transfer limitations within a fuel cell cathode, giving a doubled Tafel slope ($\alpha = 0.25$) and a first-order and half-order reaction with respect to oxygen when it was mass transport vs ionic migration controlled, respectively. Srinivasan et al.[10] applied statistical theory to both a single pore model and a thin film model, predicting $\alpha = 0.25$ at high overpotentials.

In the present paper, the activation−ohmic controlled statistical model, developed by de Levie[11] and by Srinivasan and Bockris et al.,[7,10] is employed, consistent with the lack of evidence for any sweep rate or gas flow rate dependence of our *i*/*E* data (Figures 1 and 3). [Notably, the activation−concentration controlled (diffusion-limited) case would give a similarly doubled Tafel slope and is the subject of future work.] Our model assumes that the catalyst layer consists of electronically conductive parallel cylindrical pores open to the electrolyte at one end and backed by a conductive electrode support material at the other (Figure 5a). As shown by de Levie,[11] an electrical transmission line is used to represent both the electronic and ionic resistances through this structure, as well as charge transfer along the length of the pore. Other assumptions used here include that the electrode is composed of noninterconnected pores of length *L* and radius *r*, with the pore length being greater than its diameter (2*r*), and that the porous film is chemically and physically homogeneous.

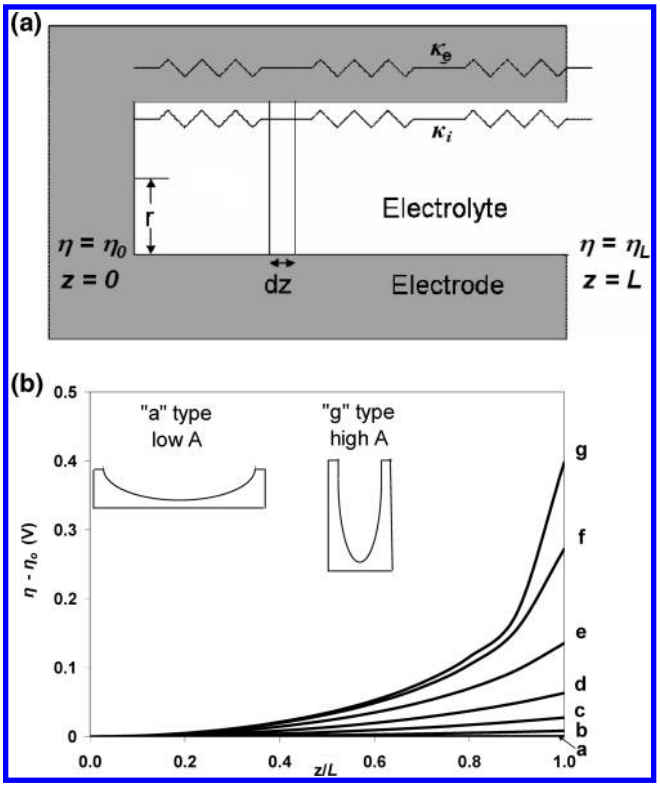

Figure 5. (a) Model of the single pore used for statistical analysis, where η = overpotential, r = pore radius, L = pore length, κ_i = ionic conductivity of electrolyte, and κ_e = electronic conductivity of electrode material. (b) Potential distribution along the pore length for various values of A: a, $A = 0.1$; b, $A = 0.4$; c, $A = 0.7$; d, $A = 1$; e, $A = 1.3$; f, $A = 1.5$; g, $A = 1.55$.

Consistent with our data, mass transport limitations in the pores are assumed to be negligible and thus the reactant/product concentrations are assumed to be constant throughout each pore. To simplify the calculations, the electronic conductivity, κ_e, of the electrode material is considered to be much larger than the ionic conductivity, κ_i, of the electrolyte in the pores, and therefore the electronic resistance can be assumed to be negligible. [It should be noted that similar results would be obtained if the reverse situation were assumed.]

With reference to Figure 5a and eq 1, and using a system of cylindrical coordinates (*z* is defined as 0 at the pore base), it can be shown that, for a simple reaction in which the first ET step is slow, the rate of an electrochemical reaction over a small length of the pore (dz), dI_z, is[7,10]

$$dI_z = 2\pi r\, dz i_o\left(\exp\left(\frac{\beta F}{RT}\eta\right) - \exp\left(\frac{-(1-\beta)F}{RT}\eta\right)\right) \quad (4)$$

where η here is the overpotential at point *z* along the pore length.

To determine the change in overpotential ($d\eta$) from $z = z$ to $z = z + dz$, eq 5, based on Ohm's law, is used[7,10]

$$d\eta = I_z \frac{dz}{\kappa_i \pi r^2} \quad (5)$$

where I_z is the current generated from $z = 0$ to $z = z$. By differentiating eq 5 with respect to *z* and then substitution with eq 4, it follows that[7,10]

$$\frac{d^2\eta}{dz^2} = \left(\frac{2}{\kappa_i r}\right) i_o\left(\exp\left(\frac{\beta F}{RT}\eta\right) - \exp\left(\frac{-(1-\beta)F}{RT}\eta\right)\right) \quad (6)$$

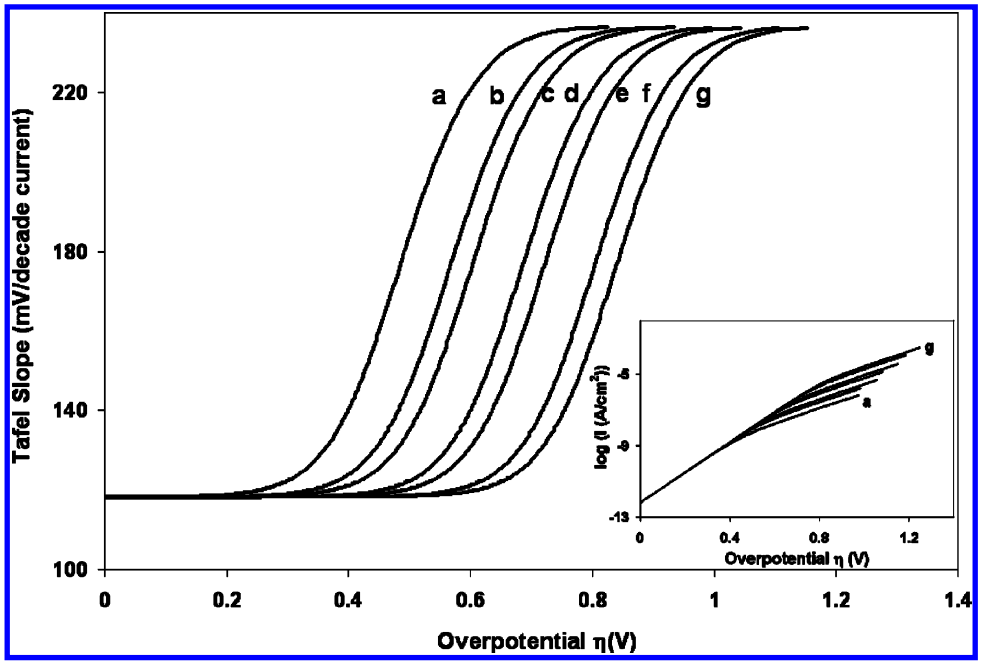

Figure 6. Tafel slope−overpotential plot with various pore conductivity values for homogeneous films at 25 °C. Inset: log *i*/*E* plot. Constant film properties are as follows: $i_o = 1 \times 10^{-6}$ A/cm^2, $L = 2 \times 10^{-3}$ cm, $r = 5 \times 10^{-5}$ cm. a, $\kappa_i = 0.01$; b, $\kappa_i = 0.05$; c, $\kappa_i = 0.1$; d, $\kappa_i = 0.5$; e, $\kappa_i = 1$; f, $\kappa_i = 5$; g, $\kappa_i = 10$ (ohm^{-1} cm^{-1}).

An analytical solution to eq 6 is obtained[7,10] when the high-field approximation of the Butler−Volmer equation is used such that the reverse reaction is negligible. Assuming $\beta = 0.5$, it follows that the total current generated through the pore from $z = 0$ to $z = L$ is[7,10]

$$I_t = \left(\frac{4RT}{LF} k_i \pi r^2\right) A \tan A \tag{7}$$

where

$$A = \left(\frac{i_o L^2 F}{2 k_i R T r}\right)^{1/2} \exp\left(\frac{\eta_o F}{4RT}\right) \tag{8}$$

Two cases of eq 8 have previously been examined,[6,7,10] where $A < 0.2$ rad and $A > 1.4$ rad (Note that A cannot be $> \pi/2$ or the current will approach infinity and eq 7 will be undefined). For $A < 0.2$ rad, and assuming that the first ET step is rate-determining, a normal Tafel slope ($\alpha = 0.5$) is then obtained.[7,10] Conversely, when $A > 1.4$, a doubled Tafel slope ($\alpha = 0.25$) is obtained. It was the purpose of our work to examine the effect of these extreme A values on α and also to determine whether intermediate Tafel slopes could be obtained ($0.25 < \alpha < 0.5$) if $0.2 < A < 1.4$.

It has been shown that[7,10] high A values (i.e., high L and i_o values) will give a large potential drop through the pore (Figure 5b), leading to a doubled Tafel slope.

$$\eta_z - \eta_o = \left(\frac{4RT}{F}\right) \ln \sec A \tag{9}$$

Alternatively, low A values (large r, κ_i, and κ_e values) will give a uniform potential distribution and therefore a normal Tafel slope (Figure 5b).

On examination of eqs 7 and 8, the four surface film parameters that most obviously influence the Tafel slope are κ_e or κ_i, L, r, and i_o. It will be shown that each of these parameters can be assigned reasonable values to produce Tafel slopes that range from normal ($\alpha = 0.5$) to doubled ($\alpha = 0.25$). As an example, Figure 6 and its inset show the effect of the ionic conductivity of the electrolyte (κ_i) on the Tafel slope at room temperature (25 °C). Assuming reasonable parameters of $L = 20$ μm, $r = 0.5$ μm, $i_o = 1 \times 10^{-6}$ A/cm^2, and $\beta = 0.5$, there is a transition from $\alpha = 0.5$ (Tafel slope = 120 mV) to $\alpha = 0.25$ (Tafel slope = 240 mV) as the overpotential (and current) increases. This transition occurs at higher overpotentials the more conductive the porous layer is, as expected. The range of potential over which this transition occurs, $\Delta\eta$, is 380 mV, independent of the film conductivity, under these room-temperature conditions. Notably, for the most conductive electrode, the Tafel slope is the normal 118 mV ($\alpha = 0.5$), even when overpotentials as high as 0.6 V are applied, while for the least conductive electrode, $\alpha = 0.25$ at overpotentials of ~0.5 V.

To examine the effect of increasing pore length (layer thickness), a similar analysis was done (Figure 7a), keeping the film parameters the same as in Figure 6 but choosing a reasonable film conductivity of 1 ohm^{-1} cm^{-1}. It is seen that the longer the pore length, the lower the overpotential at which the doubled 236 mV Tafel slope ($\alpha = 0.25$) region is reached (eq 8). As can be seen in the inset of Figure 7a, the currents in the normal Tafel region (region A) increase proportionally with the increase in active surface area (thicker films), while the currents in the doubled Tafel slope region (region B) are independent of film thickness. This is due to the fact that the apparent "penetration depth"[11] is now less than the full film thickness, such that only a constant fraction of the outer regions of the film (pore) experiences the applied potential and is involved in the electrochemical reaction.

Table 3 summarizes the predicted effect of the four film parameters on the current densities and overpotentials at which the Tafel slope starts to increase from its normal value (η_i) to when it is fully doubled (η_f) and the approximate potential range ($\Delta\eta$) over which an intermediate Tafel slope is seen, determined from eq 8 for $0.2 < A < 1.4$. It can be seen that, if the electrode conductivity or pore radius is decreased or the reaction

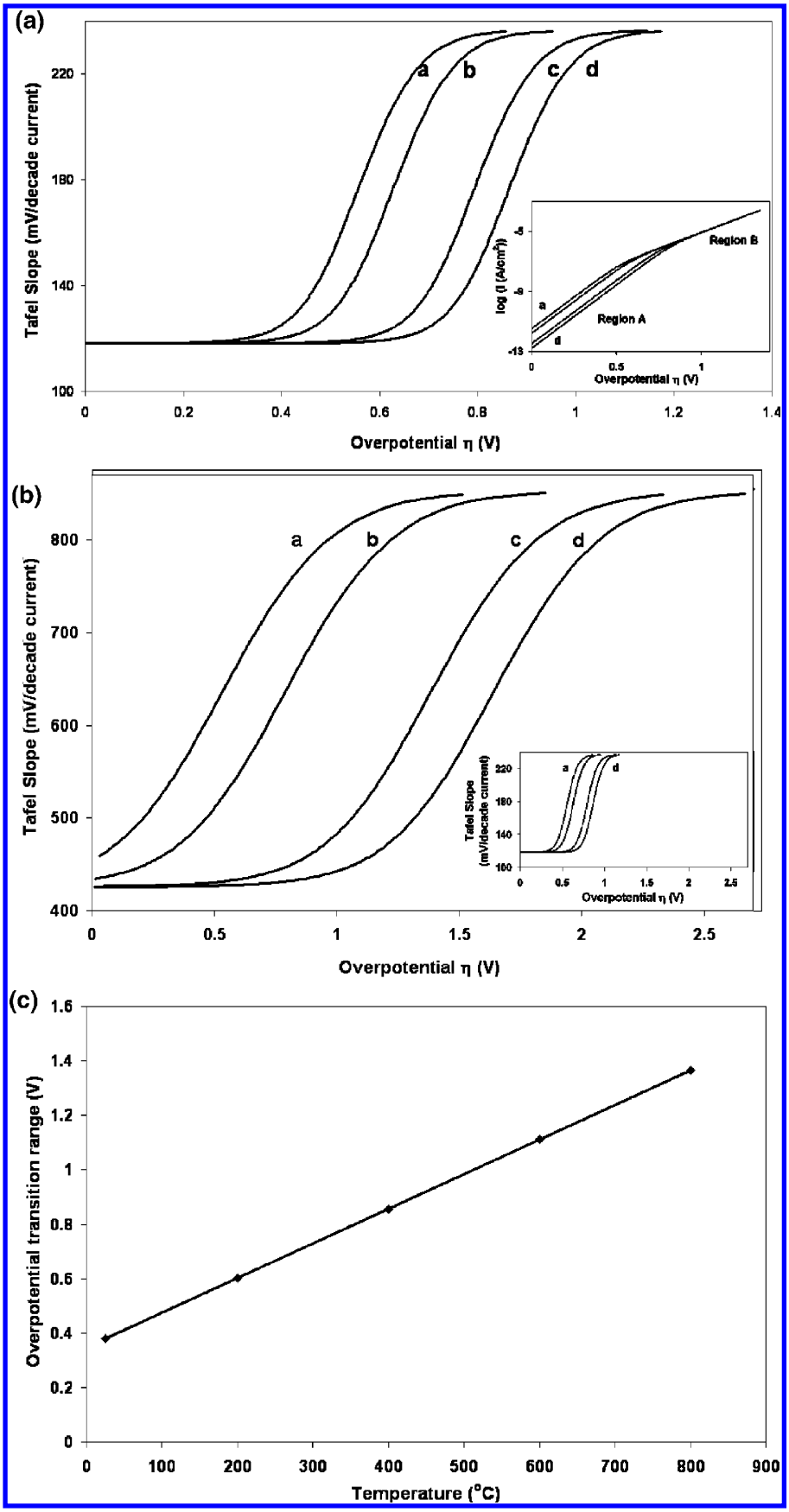

Figure 7. (a) Tafel slope−overpotential plot with various pore length values for homogeneous films at 25 °C. Inset: log *i*/*E* plot. Constant film properties are as follows: $i_o = 1 \times 10^{-6}$ A/cm^2, $\kappa_i = 1$ ohm^{-1}cm^{-1}, $r = 5 \times 10^{-5}$ cm. a, $L = 1 \times 10^{-2}$; b, $L = 5 \times 10^{-3}$; c, $L = 1 \times 10^{-4}$; d, $L = 5 \times 10^{-4}$ (cm). (b) Tafel slope−overpotential plot with various pore length values for homogeneous films at 800 °C. Inset: Tafel slope−overpotential plot at 25 °C using same parameters as at 800 °C. Constant film properties are as follows: $i_o = 1 \times 10^{-2}$ A/cm^2, $\kappa_i = 1$ ohm^{-1} cm^{-1}, $r = 5 \times 10^{-5}$ cm. a, $L = 1 \times 10^{-2}$; b, $L = 5 \times 10^{-3}$; c, $L = 1 \times 10^{-4}$; d, $L = 5 \times 10^{-4}$ (cm). (c) Overpotential transition range showing the potential range of intermediate Tafel slopes that is observed with increasing temperature.

TABLE 3: Overpotential and Current Densities at the Onset and Completion of the Doubled Tafel Slope Region (transition region, $\Delta\eta^a$ = 380 mV) at 25 °C, Based on the Statistical Pore Model[6,7,10]

pore conditions[b]	η_i (V)	i_i (A/cm^2)	η_f (V)	i_f (A/cm^2)
$i_o = 1 \times 10^{-2}$ A/cm^2	0.050	1.63×10^{-8}	0.430	3.27×10^{-6}
$i_o = 1 \times 10^{-6}$ A/cm^2	0.523	1.63×10^{-8}	0.903	3.27×10^{-6}
$i_o = 1 \times 10^{-10}$ A/cm^2	0.996	1.63×10^{-8}	1.376	3.27×10^{-6}
$\kappa_i = 0.01$ ohm^{-1} cm^{-1}	0.287	1.63×10^{-10}	0.667	3.27×10^{-8}
$\kappa_i = 0.5$ ohm^{-1} cm^{-1}	0.488	8.17×10^{-9}	0.868	1.63×10^{-6}
$\kappa_i = 10$ ohm^{-1} cm^{-1}	0.642	1.63×10^{-7}	1.021	3.25×10^{-5}
$L = 1 \times 10^{-2}$ cm	0.358	3.27×10^{-9}	0.738	6.55×10^{-7}
$L = 5 \times 10^{-3}$ cm	0.429	6.54×10^{-9}	0.809	1.31×10^{-6}
$L = 1 \times 10^{-3}$ cm	0.595	3.27×10^{-8}	0.974	6.54×10^{-6}
$L = 5 \times 10^{-4}$ cm	0.666	6.54×10^{-8}	1.046	1.31×10^{-5}
$r = 1 \times 10^{-5}$ cm	0.441	6.53×10^{-10}	0.820	1.30×10^{-7}
$r = 1 \times 10^{-4}$ cm	0.559	6.54×10^{-8}	0.939	1.31×10^{-5}
$r = 1 \times 10^{-3}$ cm	0.677	6.53×10^{-6}	1.057	1.30×10^{-3}

[a] $\Delta\eta = \eta_f - \eta_i$. η_i ($A = 0.2$) and η_f ($A = 1.4$) calculated from eq 7. Errors associated with the single and double Tafel slope approximations are <1.5%. [b] Film parameters not indicated in table are as follows: $i_o = 1 \times 10^{-6}$ A/cm^2, $\kappa_i = 1$ ohm^{-1} cm^{-1}, $L = 2 \times 10^{-3}$ cm, $r = 5 \times 10^{-5}$ cm.

TABLE 4: Overpotential and Current Densities at the Onset and Completion of the Doubled Tafel Slope Region (transition region, $\Delta\eta^a$ =1370 mV) at 800 °C, Based on the Statistical Pore Model[6,7,10]

pore conditions[b]	η_i (V)	i_i (A/cm^2)	η_f (V)	i_f (A/cm^2)
$i_o = 1 \times 10^{-2}$ A/cm^2	0.419	5.89×10^{-8}	1.786	1.18×10^{-5}
$i_o = 1 \times 10^{-6}$ A/cm^2	2.122	5.86×10^{-8}	3.489	1.18×10^{-5}
$i_o = 1 \times 10^{-10}$ A/cm^2	3.825	5.89×10^{-8}	5.192	1.18×10^{-5}
$\kappa_i = 0.01$ ohm^{-1} cm^{-1}	N/A	N/A	0.934	1.18×10^{-7}
$\kappa_i = 0.5$ ohm^{-1} cm^{-1}	0.291	2.94×10^{-8}	1.657	5.88×10^{-6}
$\kappa_i = 10$ ohm^{-1} cm^{-1}	0.844	5.89×10^{-7}	2.212	1.18×10^{-4}
$L = 1 \times 10^{-2}$ cm	N/A	N/A	1.191	2.36×10^{-6}
$L = 5 \times 10^{-3}$ cm	0.080	2.36×10^{-8}	1.447	4.71×10^{-6}
$L = 1 \times 10^{-3}$ cm	0.675	1.18×10^{-7}	2.043	2.36×10^{-5}
$L = 5 \times 10^{-4}$ cm	0.931	2.35×10^{-7}	2.298	4.71×10^{-5}
$r = 1 \times 10^{-5}$ cm	0.121	2.35×10^{-9}	1.488	4.71×10^{-7}
$r = 1 \times 10^{-4}$ cm	0.547	2.35×10^{-7}	1.914	4.71×10^{-5}
$r = 1 \times 10^{-3}$ cm	0.973	2.35×10^{-5}	2.340	4.71×10^{-3}

[a] $\Delta\eta = \eta_f - \eta_i$. η_i ($A = 0.2$) and η_f ($A = 1.4$) calculated from eq 7. Errors associated with the single and double Tafel slope approximations are <1.5%. [b] Note: film parameters not indicated in table are as follows: $i_o = 1 \times 10^{-2}$ A/cm^2, $\kappa_i = 1$ ohm^{-1} cm^{-1}, $L = 2 \times 10^{-3}$ cm, $r = 5 \times 10^{-5}$ cm.

i_o value or pore length is increased, η_i and η_f both decrease, with $\Delta\eta$ remaining constant at 380 mV under all conditions at 25 °C.

The effect of temperature is also examined here, especially in relation to the very high Tafel slopes observed for the ORR under SOFC conditions (Figure 1). Figure 7b shows the effect of pore length (film thickness) on the Tafel slope, assuming the same film parameters as in Figure 7a (but with i_o adjusted to 1×10^{-2} A/cm^2 for a temperature of 800 °C). The Tafel slope is seen to double, increasing from 425 to 850 mV (α from 0.5 to 0.25), as the overpotential is increased. However, this transition now occurs over a much larger $\Delta\eta$ range of ~1370 mV than at 25 °C (Figure 7b inset). Figure 6c shows a linear dependence of $\Delta\eta$ on temperature, and thus, intermediate α values ranging between 0.5 and 0.25 could easily be observed experimentally at high temperatures.

Table 4 summarizes the effect of the electrode parameters on η_i, η_f, and $\Delta\eta$, all at 800 °C (cf. 25 °C data in Table 3). It can be seen that as κ_i or r are decreased, or as i_o or L are increased, η_i and η_f both decrease, while the $\Delta\eta$ value remains at 1370 mV. As expected, the currents are also higher at η_i and η_f due to the increased temperature and the resulting higher i_o values (assumed to be 1×10^{-2} A/cm^2 vs 1×10^{-6} A/cm^2 at 25 °C).

It is clear from Figure 1 that the α values are <0.5 for the ORR on porous LSM−YSZ composite cathodes and that the lower pore radii gave an α value of 0.24 (vs 0.35 for larger pores; Figure 1a). This agrees with the predictions discussed above (eq 8). It was also found that, even after IR compensation, the log i/η plots were sometimes curved, perhaps indicating that the data are being collected in the transition region, when α is changing from 0.5 to 0.25.

As well, Figure 1b shows that the Tafel plots obtained for 10 and 15 μm thick LSM−YSZ composite layers give α values of 0.37 and 0.31, respectively, showing that α = 0.25 will generally be seen at lower overpotentials at thick, vs at thin,

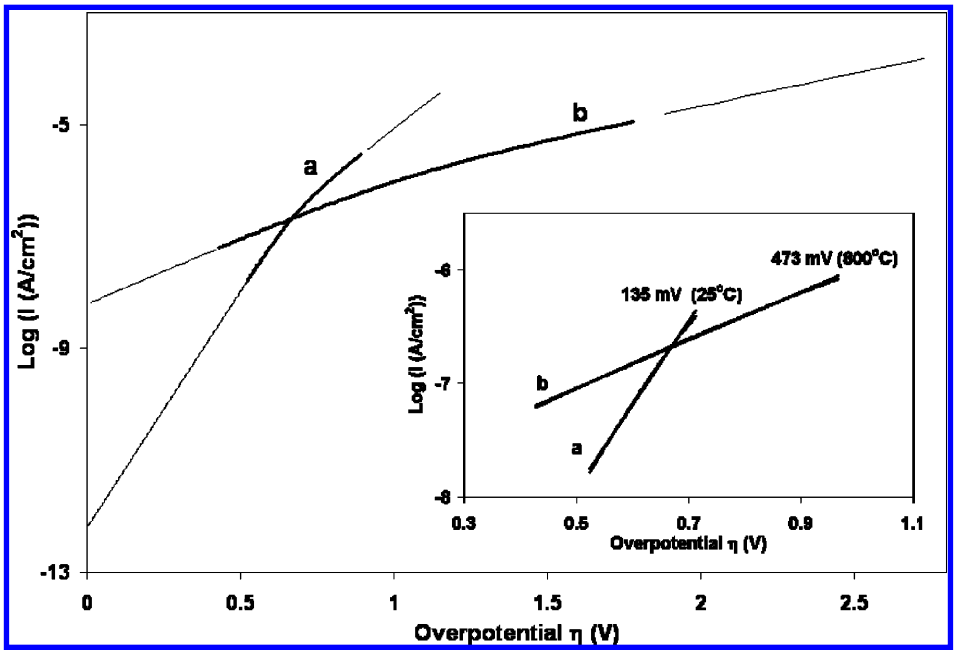

Figure 8. Tafel plot showing the overpotential transition range from a single to double Tafel slope. Constant film properties are as follows: $L = 2 \times 10^{-3}$ cm, $\kappa_i = 1$ ohm^{-1} cm^{-1}, $r = 5 \times 10^{-5}$ cm. a, $i_o = 1 \times 10^{-6}$ A/cm^2 at 25 °C; b, $i_o = 1 \times 10^{-2}$ A/cm^2 at 800 °C.

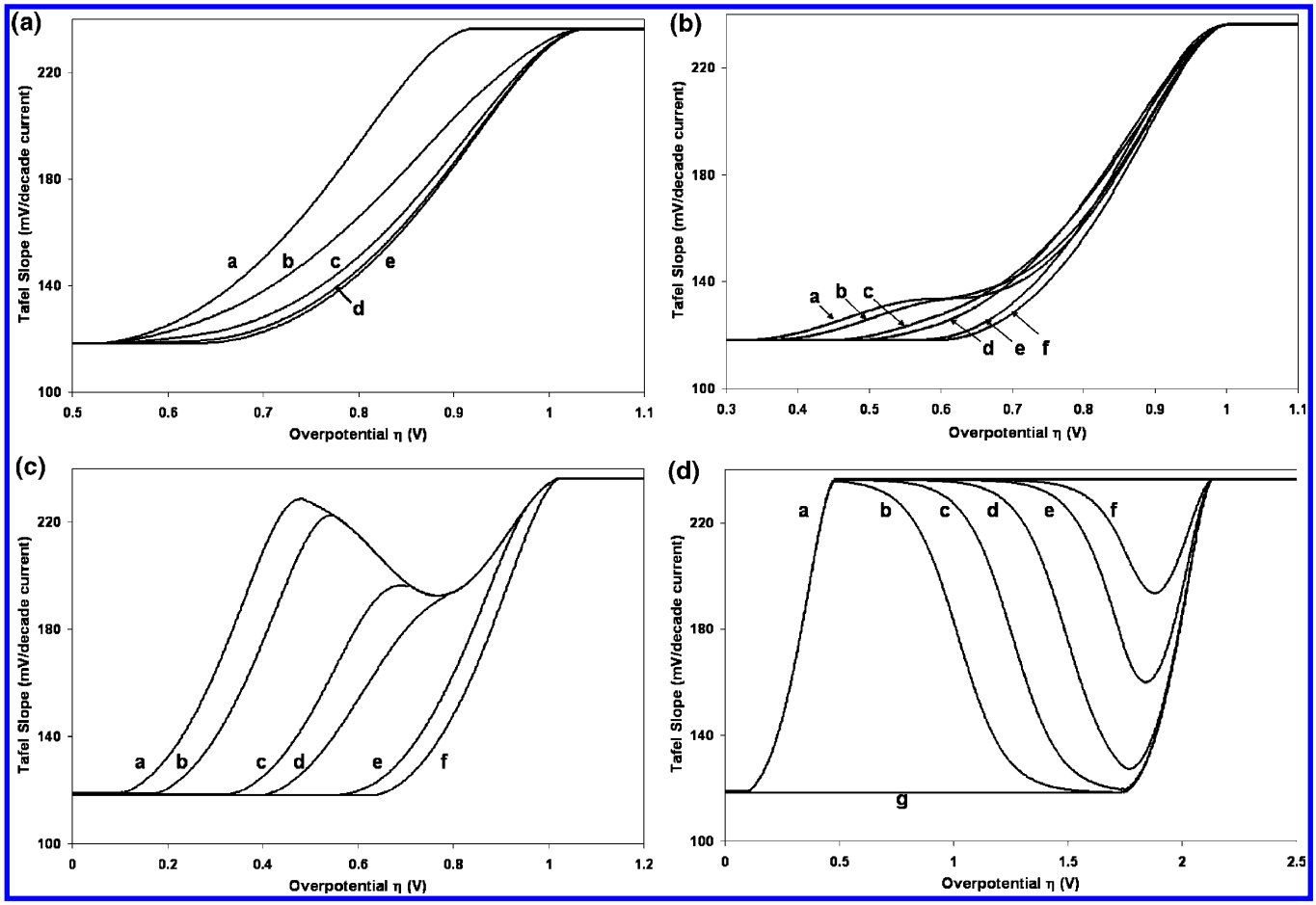

Figure 9. (a) Tafel slope−overpotential plot with various pore radius ratios at 25 °C for a nonhomogeneous pore structure. Constant parameters are as follows: $i_o = 1 \times 10^{-6}$ A/cm^2, $\kappa_i = 1$ ohm^{-1} cm^{-1}, $L = 2 \times 10^{-3}$ cm. a, $r = 1 \times 10^{-4}$; b, $r = 1 \times 10^{-4}$, 1×10^{-3} (20:1); c, $r = 1 \times 10^{-4}$, 1×10^{-3} (4:1); d, $r = 1 \times 10^{-4}$, 1×10^{-3} (1:1); e, $r = 1 \times 10^{-3}$ (cm). (b) Tafel slope−overpotential plot with various pore conductivity values at 25 °C for a nonhomogeneous pore structure. Constant parameters are as follows: $i_o = 1 \times 10^{-6}$ A/cm^2, $r = 5 \times 10^{-5}$ cm, $L = 2 \times 10^{-3}$ cm. a, $\kappa_i = 0.05$, 10 (1:1); b, $\kappa_i = 0.1$, 10 (1:1); c, $\kappa_i = 0.5$, 10 (1:1); d, $\kappa_i = 1$, 10 (1:1); e, $\kappa_i = 5$, 10 (1:1); f, $\kappa_i = 10$ (ohm^{-1} cm^{-1}). (c) Tafel slope−overpotential plot with various pore length values at 25 °C for a nonhomogeneous pore structure. Constant parameters are as follows: $i_o = 1 \times 10^{-6}$ A/cm^2, $r = 5 \times 10^{-5}$ cm, $\kappa_i = 1$ ohm^{-1} cm^{-1}. a, $L = 1 \times 10^{-1}$, 5×10^{-4} (1:1); b, $L = 5 \times 10^{-2}$, 5×10^{-4} (1:1); c, $L = 1 \times 10^{-2}$, 5×10^{-4} (1:1); d, $L = 5 \times 10^{-3}$, 5×10^{-4} (1:1); e, $L = 1 \times 10^{-3}$, 5×10^{-4} (1:1); f, $L = 5 \times 10^{-4}$ (cm). (d) Tafel slope−overpotential plot with various pore length ratios at 25 °C for a nonhomogeneous pore structure. Constant parameters are as follows: $i_o = 1 \times 10^{-6}$ A/cm^2, $r = 5 \times 10^{-5}$ cm, $\kappa_i = 1$ ohm^{-1} cm^{-1}. a, $L = 1 \times 10^{-1}$; b, $L = 1 \times 10^{-1}$, 1×10^{-8} (1:1); c, $L = 1 \times 10^{-1}$, 1×10^{-8} (1:4); d, $L = 1 \times 10^{-1}$, 1×10^{-8} (1:40); e, $L = 1 \times 10^{-1}$, 1×10^{-8} (1:400); f, $L = 1 \times 10^{-1}$, 1×10^{-8} (1:4000); g, $L = 1 \times 10^{-8}$ (cm).

catalyst layers (Figure 7b). At higher overpotentials, even thin LSM−YSZ cathodes with large diameter pores will give α_c values of 0.25, as predicted by Figure 7a,b.

2.2.2. Tafel Slopes between Normal and Doubled ($0.25 < \alpha < 0.5$). In the experimental results shown in Figures 1 and 3, stable Tafel regions over relatively wide potential ranges, with α values between 0.5 and 0.25, are seen. In fact, this is a fairly common situation in the literature; e.g., slopes of ∼200 mV were reported for the room-temperature reduction of H_2O_2 on porous Pt,[19] while ∼130 to 200 mV slopes were obtained for O_2 evolution at various electrode surfaces.[20] However, the porous electrode literature[5−7,11,12] and the treatment above (eqs 4−9) do not lead to this prediction, giving only either the normal Tafel slope or its doubled value, with a transition region, $\Delta\eta$, over which the slope changes from one to the other. The analyses below demonstrate how the properties of porous electrodes can help to explain these observations.

2.2.2.1. Effect of Insufficiently High Polarization. Figure 8 shows some theoretical Tafel plots at 25 and 800 °C (curve b), with the i_o values adjusted for temperature and using constant pore characteristics of $r = 0.5$ μm, $\kappa_i = 1$ ohm^{-1}cm^{-1}, and $L = 20$ μm. The inset to Figure 8 shows the same data, but focusing only on the $\Delta\eta$ region, as would be the case if η had not been extended to a sufficiently high value. Figure 8 indicates that slopes of 135 and 473 mV at 25 and 800 °C, respectively, could be erroneously obtained from these data. These slopes translate to transfer coefficient values of 0.44 and 0.45, respectively. Therefore, the measurement of Tafel slopes from a transition region, which may appear to be linear, may be the explanation for some of the reported Tafel slopes that are larger than 118 mV (room temperature) but not fully doubled in value. Efforts to establish whether this is the case experimentally would entail the application of higher overpotentials. Unfortunately, this is often not possible or practical, due to the very high currents that may be generated or due to the onset of other electrochemical reactions.

2.2.2.2. Nonuniform Porous Electrodes. Another explanation for Tafel slopes that are between normal and doubled (α between 0.5 and 0.25) is the nonuniformity of porous electrode layer architectures, including nonuniform electrode thickness, pore radius, or conductivity, thus contravening the assumed electrode homogeneity. This heterogeneity is seen clearly in Figure 4 for the Co-based ORR catalysts explored in Figure 3. For high temperature SOFCs (Figures 1 and 2), the electrocatalytic layers are normally deposited by physically mixing and then screen-printing the powdered mixtures onto a solid electrolyte surface.

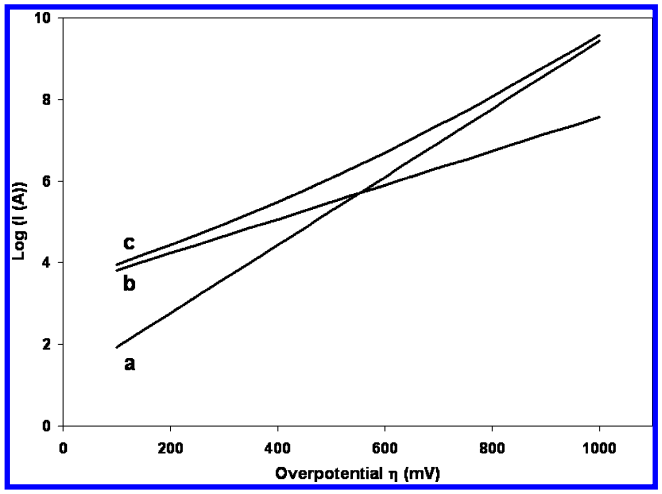

Figure 10. Tafel plot showing the curves for a nonporous electrode, porous electrode, and mixed electrode with regions of porosity (refer to eq 10). a, nonporous electrode where $x = 1$, $y = 0$ ($\alpha = 0.5$); b, porous electrode where $x = 0$, $y = 1$ ($\alpha = 0.25$); c, mixed electrode where $x = 0.1$, $y = 1$.

Thus, a random mixture of pore diameters and lengths will result (Figure 2), and some regions may also have a much different conductivity than others.

Figure 9a shows the Tafel slopes that would be obtained for porous electrode layers consisting of pores of two different radii and variable distributions. It is seen that $\Delta\eta$ is now significantly broader (curves b and c) vs the case when all of the pore radii are the same (curve a) (Tables 3 and 4). This results in a wider $\Delta\eta$ range over which an apparent intermediate Tafel slope (α between 0.25 and 0.5) region is obtained. The same effect is observed if the electrodes are assumed to contain regions of different inherent activity, i.e., two different i_o values. In the case of variable conductivity within the electrode, Figure 9b shows that intermediate Tafel slopes, with values between 118 and 236 mV over a range of overpotentials, can be obtained.

Interestingly, extreme variations in the pore length of different regions of a porous electrode layer can lead to Tafel slopes that either increase or decrease with η. Figure 9c,d shows examples of this effect for films containing a 1:1 ratio of regions with pore lengths differing by a factor of 100. Figure 9c shows that an η range of ~200 mV exists over which the Tafel slope is constant at ~190 mV. In Figure 9d, it can be seen that, depending on the assumed porous film properties, the Tafel slopes can transition from normal ($\alpha = 0.5$) to doubled ($\alpha = 0.25$) and then back to normal again, as the overpotential is increased.

An alternative approach was also used to understand the effect of nonuniform porous film properties on the observed Tafel slopes. Part of the electrode was assumed to be coated with a region that behaves like a nonporous surface film exhibiting "normal" Tafel slope behavior ($\alpha = 0.5$), with the remainder being porous, with $\alpha = 0.25$ (eq 10).

$$i = xi_o\left(\exp\left(\frac{F}{2RT}\eta\right) - \exp\left(\frac{-F}{2RT}\eta\right)\right) + yi_o\left(\exp\left(\frac{F}{4RT}\eta\right) - \exp\left(\frac{-F}{4RT}\eta\right)\right) \quad (10)$$

If it is assumed that x is 0.1 and y is 1, i.e., that ~90% of the electrode contains long and narrow pores that would demonstrate doubled Tafel slopes, Figure 10 (curve c) demonstrates that intermediate Tafel slopes could indeed be obtained, with values between those for a nonporous and fully porous electrode. It is also seen that, at low currents, the Tafel slope would give an α value of 0.25, while at higher overpotentials, $\alpha = 0.5$. This is analogous to what is shown in Figure 9c,d.

It is clear that, if the morphology and structure of a porous electrode are nonuniform, a wide range of Tafel slopes, having α values anywhere between 0.5 and 0.25, could be seen over different overpotential ranges. Also, as the temperature of the system increases, these overpotential ranges will broaden. Thus, based on the present work, reliable mechanistic analysis based on measured α values can only be achieved using experimental data collected on model (uniform and nonporous) electrode materials.

Summary

This work has focused on understanding the factors responsible for anomalously high Tafel slopes (or for transfer coefficients, α, having values <0.5), with a specific focus on the oxygen reduction reaction (ORR) under both low- and high-temperature fuel cell conditions. It is shown that, when the predicted α value is 0.5, as the electrocatalyst particles (and pores) are made smaller or as the electrode layers are made thicker (pores become longer), the α value can become as small as 0.25. In other cases, α remains constant at a value between 0.25 and 0.5. Assuming that the symmetry coefficient, β, is 0.5, these small α values cannot be explained using any of the commonly encountered adsorption isotherms for reactants and intermediates. However, models related to the effect of porous electrode structures do exist in the literature to explain doubled Tafel slope values, arising from a distribution of potential in the electrode pores.

In the present work, a standard porous electrode model was used, showing that variables such as the exchange current, pore radius, pore length, and electrode or electrolyte conductivity are the key factors in giving low α values, especially as the overpotential/currents are increased. It is also demonstrated that the potential range over which α transitions from 0.5 to 0.25 is temperature dependent. At high temperatures, e.g. >600 °C, applicable for solid oxide fuel cell applications, the transition region is very broad (~1.3 V), while under room temperature conditions, this range is 0.35−0.4 V. Particularly at high temperatures, this large transition range can be misinterpreted as a valid Tafel region of intermediate slope, giving apparent α values of between 0.25 and 0.5.

It is also shown here that nonuniform activity, pore distribution, thickness, or conductivity of the porous electrode material may lead to intermediate α values, thus making mechanistic analysis from Tafel slopes very complex. In some cases, the theoretical predictions show that the Tafel slope can increase and then decrease again with increasing overpotential. Overall, this study shows that a reliable mechanistic analysis can only be carried out on nonporous electrodes or at porous electrode of the appropriate morphology.

Acknowledgment. This work was supported by The Alberta Energy Research Institute (AERI) through the Coordination of University Research for Synergy and Effectiveness (COURSE) program and the Natural Science and Engineering Research Council of Canada (NSERC). The authors also thank Versa Power Systems for the provision of materials and Dr. P. Vanysek (NIU) for useful discussions.

List of Symbols

F = Faraday constant (96485 C/mol)
I = current (A)

I_o = exchange current (A)
i = current density (A/cm^2)
L = pore length (cm)
i_o = exchange current density (A/cm^2)
R = gas constant (8.31451 J/Kmol)
r = pore radius (cm)
r_{rds} = number of electrons transferred during the rate determining step
T = temperature (K)
z = distance coordinate along the pore length
α_{mech} = mechanistic transfer coefficient
α = experimentally measured transfer coefficient
β = symmetry coefficient
γ = number of electrons transferred before the rate determining step
η = overpotential (V)
κ_i = ionic conductivity (ohm^{-1} cm^{-1})
κ_e = electronic conductivity (ohm^{-1} cm^{-1})
ν = stoichiometry of the rate-determining step

References and Notes

(1) Bockris, J. O. M.; Reddy, A. K. N. *Modern Electrochemistry: An Introduction to an Interdisciplinary Area*; Plenum Publishing Corporation: New York, 1977; Vol. 1.

(2) Bard, A. J.; Faulkner, L. R. *Electrochemical Methods: Fundamentals and Applications*, 2nd ed.; John Wiley & Sons: New York, 2001; Vol. 1.

(3) Co, A. C.; Xia, S. J.; Birss, V. I. *J. Electrochem. Soc.* **2005**, *152*, A570.

(4) Bockris, J. O. M.; Khan, S. U. M. *Surface Electrochemistry: A Molecular Level Approach*; Plenum Press: New York and London, 1993.

(5) Tilak, B. V.; Venkatesh, S.; Rangarajan, S. K. *J. Electrochem. Soc.* **1989**, *136*, 1977.

(6) Tilak, B. V.; Yeo, R. S.; Srinivasan, S. Electrochemical Energy Conversion-Principles. In *Comprehensive Treatise of Electrochemistry: Electrochemical Energy Conversion and Storage*; Bockris, J. O. M., Conway, B. E., Yeager, E., White, R. E., Eds.; Plenum Press: New York, 1981; Vol. 3, p 39.

(7) Bockris, J. O. M.; Srinivasan, S. *Fuel Cells: Their Electrochemistry*; McGraw-Hill: New York, 1969.

(8) Austin, L. G.; Lerner, H. *Electrochim. Acta* **1964**, *9*, 1469.

(9) Perry, M. L.; Newman, J.; Cairns, E. J. *J. Electrochem. Soc.* **1998**, *145*, 5.

(10) Srinivasan, S.; Hurwitz, H. D.; Bockris, J. O. M. *J. Chem. Phys.* **1967**, *46*, 3108.

(11) de Levie, R. Electrochemical Respose of Porous and Rough Electrodes. In *Advances in Electrochemistry and Electrochemical Engineering*; Delahay, P., Ed.; John Wiley & Sons: New York, 1967; Vol. 6, p 329.

(12) Chizmadzhev, Y. A.; Chirkov, Y. G. Porous Electrodes. In *Comprehensive Treatise of Electrochemistry, Electrodics: Transport*; Yeager, E., Bockris, J. O. M., Conway, B. E., Sarangapani, S., Eds.; Plenum Press: New York and London, 1983; Vol. 6, p 317.

(13) Co, A. C. Ph.D. Thesis, University of Calgary, 2005.

(14) Winkler, J.; Hendriksen, P. V.; Bonanos, N.; Mogensen, M. *J. Electrochem. Soc.* **1998**, *145*, 1184.

(15) Sirk, A. H. C.; Cambell, S. A.; Birss, V. I. *Electrochem. Solid State Lett.* **2005**, *8*, A104.

(16) Sirk, A. H. C. Ph.D. Thesis, University of Calgary, 2004.

(17) Sirk, A. H. C.; Campbell, S.; Birss, V. I. Manuscript in preparation.

(18) Co, A. C.; Birss, V. I. *J. Phys. Chem. B*, manuscript accepted for publication.

(19) Huang, J. C.; Sen, R. K.; Yeager, E. *J. Electrochem. Soc.* **1979**, *126*, 786.

(20) Hoare, J. P. *The Electrochemistry of Oxygen*; Interscience Publishers: New York, 1968.